

Electrochemical and statistical analyses of the combined effect of air-entraining admixture and micro-silica on corrosion of reinforced concrete



Anis Ghanei^{a,*}, Hamid Eskandari-Naddaf^{a,*}, Togay Ozbakkaloglu^b, Ali Davoodi^c

^a Department of Civil Engineering, Hakim Sabzevari University, Sabzevar, Iran

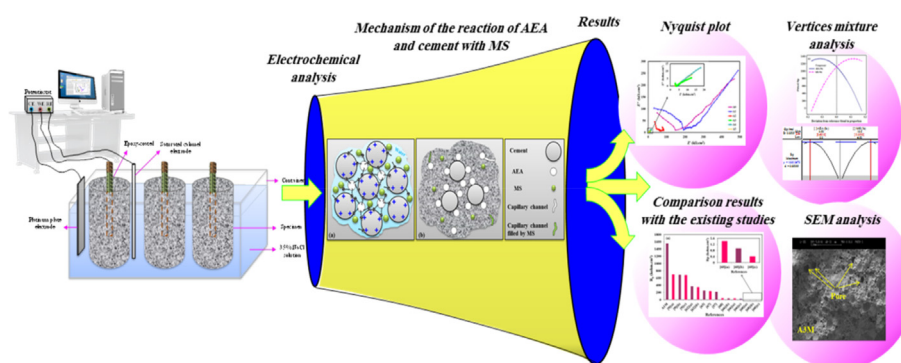
^b Ingram School of Engineering, Texas State University, San Marcos, TX, USA

^c Materials and Metallurgical Engineering Department, Ferdowsi University of Mashhad, Iran

HIGHLIGHTS

- Combined effect of AEA and MS on corrosion of reinforced concrete is studied.
- Using up to 0.7% AEA and 10% MS as cement replacement improved corrosion resistance.
- High content of AEA has a negative effect on corrosion behavior of reinforced concrete.
- Mixture method can appropriately find the optimal and influential components.

GRAPHICAL ABSTRACT



ARTICLE INFO

Article history:

Received 20 April 2020

Received in revised form 16 August 2020

Accepted 30 August 2020

Available online 22 September 2020

Keywords:

Air-entraining admixture

Micro-silica

Electrochemical analysis

Extreme vertices mixture method

ABSTRACT

This study aims to clarify the combined effect of air-entraining admixture (AEA) and micro-silica (MS) on the structure of cement mortar to improve the corrosion behavior of the resulting reinforced concrete. Open circuit potential (OCP), electrochemical impedance spectroscopy (EIS), and linear polarization resistance (LPR) tests were conducted on specimens after placing them in a 3.5% chloride solution. Scanning electron microscopy (SEM) imaging was also performed to characterize the surface porosity of the specimens. In addition, a comparison study with existing studies in the literature was performed to evaluate the accuracy of the obtained results. Moreover, a statistical analysis was performed using the extreme vertices mixture method to obtain the optimal value and contribution of each influential component. The results of the experiments indicate that using up to 0.7% AEA and 10% MS as a cement replacement provides the optimal combination among the mixes of the present study, as well as in comparison with existing studies. The results of the statistical analysis indicate that the optimal responses (i.e., maximum concrete resistance against penetration (R_c), electrical charge transfer resistance of the reinforcing bar (R_{ct}), polarization resistance (R_p), and minimum corrosion rate (CR)) are achieved for dosages of AEA and MS in the ranges of 0.60% to 0.69% and 9.31% to 9.40%, respectively. The results also show that the AEA dosage is more influential in improving the R_c , R_{ct} , and R_p , whereas MS dosage is more influential in reducing the CR.

© 2020 Elsevier Ltd. All rights reserved.

1. Introduction

Today, micro-silica (MS) is used in combination with different admixtures to improve the properties of concrete [1–6]. For

* Corresponding authors.

E-mail addresses: Anisghanei.civil@yahoo.com (A. Ghanei), H.eskandari@hsu.ac.ir (H. Eskandari-Naddaf).

instance, using MS and nano-silica improves the microstructure of cement mortar [5], which increases the concrete resistance against the penetration of water, as well as sulfate, carbonation, and chloride ions. The optimal values of 10% MS and 2% nano-silica can protect concrete against corrosion and increase its resistance against destructive ion attack [6]. Recent research has also suggested that using 10% MS along with other pozzolanic materials, such as fly ash [7,8] and metakaolin [9], results in higher compressive strength compared to lower dosages and reduces the permeability of concrete by decreasing the size of capillary pores [10]. Other properties established by MS in concrete include increased durability and corrosion resistance [11,12], as well as resistance against the attack of chemical factors and reduced permeability in the presence of air-entraining admixture (AEA) [13–17]. Furthermore, an optimal amount of AEA improves the mechanical properties, salt scaling resistance, and transport properties of concrete [18,19]. Moreover, chloride ion diffusion testing conducted on concrete containing both MS and fly ash has shown that using a proper AEA dosage absorbs chloride ions to C-S-H layers. This, in turn, improves the microstructure of cement mortar due to pozzolanic reactions, resulting in good resistance against chloride ion diffusion before and after freeze–thaw cycles [20,21].

One of the most significant durability factors of reinforced concrete is corrosion resistance, which is usually measured using two groups of general methods. The first group includes open circuit potential (OCP) and electrical resistance, explaining the corrosion probability and the concrete resistance against the penetration of destructive ions, respectively. The second category includes more efficient techniques, such as electrochemical impedance spectroscopy (EIS), linear polarization resistance (LPR), and Tafel polarization, which are used to obtain more accurate results. For instance, performing three corrosion tests of OCP, LPR, and Tafel polarization in a 3.5% chloride solution on reinforced concrete containing 10% ground granulated blast-furnace slag and 2% calcium nitrate corrosion inhibitor has shown improved mechanical properties and can reduce the corrosion of reinforcing bars [22]. In addition, the powerful EIS has been used in different studies [23–26] to investigate corrosion behavior, concrete resistance against ion penetration (R_c), electrical charge transfer resistance (R_{ct}) of the reinforcing bar embedded in concrete, surface porosity of concrete (n_c), and surface porosity of the reinforcing bar (n_{dl}). Furthermore, the electrochemical methods of OCP, EIS, and LPR have been used to investigate the simultaneous effect of MS, fly ash, and metakaolin on the corrosion behavior of concrete [9]. The results showed that the simultaneous use of these admixtures prevented the transfer of ions by increasing electrical resistance while creating negligible changes in corrosion potential, polarization resistance (R_p), corrosion current (i_{corr}), and the impedance between the reinforcement and the concrete.

Obtaining the optimal dosages of simultaneously used admixtures can significantly improve the mechanical properties, durability, and corrosion behavior of concrete. For this purpose, recently conducted studies have used some optimization and prediction methods [27,28], such as the Taguchi [29,30], Factorial [31,32], and mixture [33–36] techniques. Among these different methods, the utilization of the extreme vertices mixture method has attracted noticeable attention. For instance, a study used the extreme vertices mixture method to simplify the mixing ratios of different mineral compounds in concrete [35]. Another study utilized this method to evaluate the fresh properties of concrete and to assess different sand types in the mixing proportions [36]. The results indicated that the use of derived mathematical models in such methods provides flexibility to optimize the intended responses.

A review of the literature reveals the importance of optimizing the dosages of AEA and MS and of investigating their combined

effect on reinforced concrete corrosion. The combined effect of AEA and MS on the corrosion of reinforced concrete using different electrochemical techniques has not yet been addressed in the literature. The present study addresses this important gap by investigating the corrosion behavior of reinforced concrete containing AEA and MS using OCP, EIS, and LPR. A comparison of the present study with existing studies was also performed to evaluate the efficiency of the results. Moreover, a statistical analysis was conducted using the extreme vertices mixture method to optimize the dosages of AEA and MS and to determine the percent contribution of each effective factor.

2. Materials and specimen preparation

In this project, cement, fine and coarse aggregates, AEA, MS and super-plasticizer were used in mix designs to produce the test specimens. The cement was an ordinary Portland cement (CEM II 52.5 N) [37] procured in Torbat cement factory. Generally, using air-entraining admixture reduces the strength and durability of concrete, leading to a decreased corrosion resistance [38,39]. It appears using a high cement grade of 52.5 MPa that is being produced at a cost almost similar to other grades is more economical [40] and is required for wide construction, where corrosion resistance is essential [41–44].

The chemical composition and physical properties of the cement are listed in Tables 1 and 2, respectively. As can be observed in Table 2, the autoclave expansion value was 0.12%, while the ASTM C150 [45] limits the autoclave expansion of cement by 0.8%. Accordingly, the expansion of the utilized cement, which usually occurs due to the presence of free lime or magnesia is very trivial as compared to the limit set by the ASTM Standard.

The chemical analysis and physical properties of MS are listed in Table 3. A polycarboxylate-based super-plasticizer admixture satisfying the requirements of ASTM C494 [46] was also employed in mix designs with MS to achieve appropriate workability. In order to avoid errors in the experimental results that may be caused by the air entrainment of super-plasticizer, a constant amount of this admixture was used in all mixes containing MS; thus, the produced air content could be ignored.

The fine and coarse aggregates used in the mix designs were proportioned according to ASTM C136 [47] in order to have an appropriate sieve analysis and an adequate strength. Different dosages of AEA (i.e. 0, 0.7, 1.4, 2.1, 2.8 and 3.5% by weight of binder) were also considered in mix designs in accordance with ASTM C260 [48]. AEA had an exact gravity of 1.01 g/cm³ and a pH of approximately 7.

Since previous research [15,17,49] reported using 10% MS significantly improves the corrosion behavior, the replacement ratio of MS (by weight of the cement) was set to 10% in half of the mixes.

Table 4 shows the details of the mix designs used to produce a total of 12 cylindrical specimens with a diameter of 100 mm and a height of 150 mm. All mixes were blended using a concrete mixer for approximately 4 min until a uniform consistency was achieved. Then, the molds were filled with concrete and appropriately vibrated using a vibrating table. A St37 steel reinforcing bar, with a diameter of 10 mm and a length of 150 mm, was placed in the middle of each specimen. After 24 h, the specimens were demolded and wet-cured for 28 days in a curing tank. Finally, the reinforced concrete specimens were exposed to 3.5% NaCl solution for 2 weeks followed by another 2 weeks in dry conditions.

Fig. 1 illustrates the actual and schematic views of the exposure of specimens to the corrosive environment. As can be observed, the top 50 mm of the rebar was epoxy-coated to be protected against corrosion, whereas the embedded part of the reinforcing bar was unprotected.

Table 1
Chemical composition of Portland cement.

Ingredient	SiO ₂	Al ₂ O ₃	Fe ₂ O ₃	CaO	MgO	K ₂ O	SO ₃	Na ₂ O	LOI
%	21.54	4.95	3.82	63.24	1.55	0.75	2.43	0.48	1.24

Table 2
Physical properties of Portland cement.

	Blain (cm ² /g)	Initial setting time (min)	Final setting time (min)	Autoclave.Expansion (%)
Cement	3083	119	218	0.12
Allowable scale	Min ≥ 2800	Min 45 ≥	Max ≤ 360	Max ≤ 0.8

Table 3
Chemical analysis and physical properties of MS.

Chemical analysis	Value (%)
SiO ₂	96.4
Al ₂ O ₃	1.32
Fe ₂ O ₃	0.87
CaO	0.49
MgO	0.97
Na ₂ O	0.31
K ₂ O	1.01
SO ₃	0.1
Physical properties	Value
Colour	white
Specific Surface Area (m ² /gr)	20–25
Density (gr/cm ³)	1.9
Particle size (nm)	229
Particle shape	Globular
Structure	Amorphous
Bulk density/kg/cm ³	300–500

3. Electrochemical measurements

Electrochemical measurements (i.e. OCP, EIS and LPR tests) were performed using Gill AC automated potentiostat (ACM instruments). OCP testing is one of the easy and preliminary electrochemical methods to measure the corrosion status of reinforced concrete [50]. The OCP was measured using a saturated calomel electrode (SCE) as a reference.

EIS is a powerful tool to assess the reinforced concrete structures in order to detect corrosion occurrences [51–54]. It is known as a technique that provides corrosion rate (CR) in the frequency domain [55–58]. Accordingly, the EIS measurements of the present study were conducted in a frequency range between 30 kHz and 0.1 Hz. Then, the obtained values were investigated using the EIS Spectrum Analyser software [59].

LPR is a method that measures the CR of the reinforcing bars in concrete [55,56,60]. Polarization resistance (R_p) is defined as the

Table 4
Details of mix designs used to produce the test specimens.

Mix No.	Water(kg/m ³)	Cement(kg/m ³)	Water/Binder	Aggregates(kg/m ³)	AEA(kg/m ³)	MS(kg/m ³)	Super-plasticizer(kg/m ³)	Hardened density (kg/m ³)
A0	278	555	0.5	1586	0	0	0	2274
A1	278	555	0.5	1586	3.9	0	0	2269
A2	278	555	0.5	1586	7.8	0	0	2264
A3	278	555	0.5	1586	11.7	0	0	2260
A4	278	555	0.5	1586	15.5	0	0	2255
A5	278	555	0.5	1586	19.4	0	0	2250
A0M	278	500	0.5	1586	0	55	8	2308
A1M	278	500	0.5	1586	3.9	55	8	2303
A2M	278	500	0.5	1586	7.8	55	8	2298
A3M	278	500	0.5	1586	11.7	55	8	2293
A4M	278	500	0.5	1586	15.5	55	8	2293
A5M	278	500	0.5	1586	19.4	55	8	2289

*AEA: Air-3entraining admixture, MS: Micro-silica

ratio between the potential variation and the current variation. The R_p can be related to the corrosion current density (i_{corr}) using the Stern–Geary equation (Eq. (1)) [40]:

$$i_{corr} = \frac{B}{R_p} \quad (1)$$

Where, B is a constant value related to the anodic and cathodic Tafel slopes (β_a and β_c), and it is determined using Eq. (2):

$$B = \frac{B_a B_c}{2.303(B_a + B_c)} \quad (2)$$

The B value for reinforcing bar–concrete systems is in the range of 25 to 52 mV, and it is usually taken as 26 mV [61], which is also adopted in the current study. All measurements were performed under the same conditions and at a temperature of approximately 25 °C. The experimental setup for the electrochemical tests is schematically shown in Fig. 2.

4. Results and discussion

4.1. OCP measurements

The OCP test shows the corrosion probability of reinforcing bars, with more negative OCP values indicating a higher corrosion probability. OCP values that are less negative than -126 mV/SCE indicate that the probability of corrosion is <10%. For values more negative than -276 mV/SCE, it can be stated that the probability of corrosion is more than 90%, while values between -126 and -276 mV/SCE indicate uncertain corrosion [62]. As seen in Fig. 3, the OCP values for the mixes without MS (A0–A5) fluctuated, and their variations did not follow a specific trend. Moreover, these OCP values were all more negative than -276 mV/SCE, indicating that their corrosion probability was more than 90%. On the other hand, for the mixes with MS (A0M–A5M), there was a significant increase in OCP value (decrease in corrosion probability), with

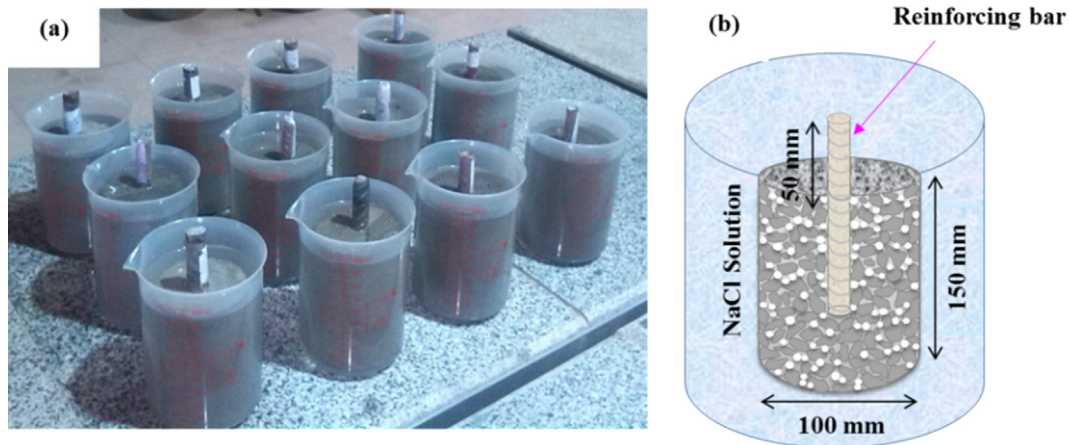


Fig. 1. Cylindrical specimens exposed to a corrosive environment: (a) actual and (b) schematic views.

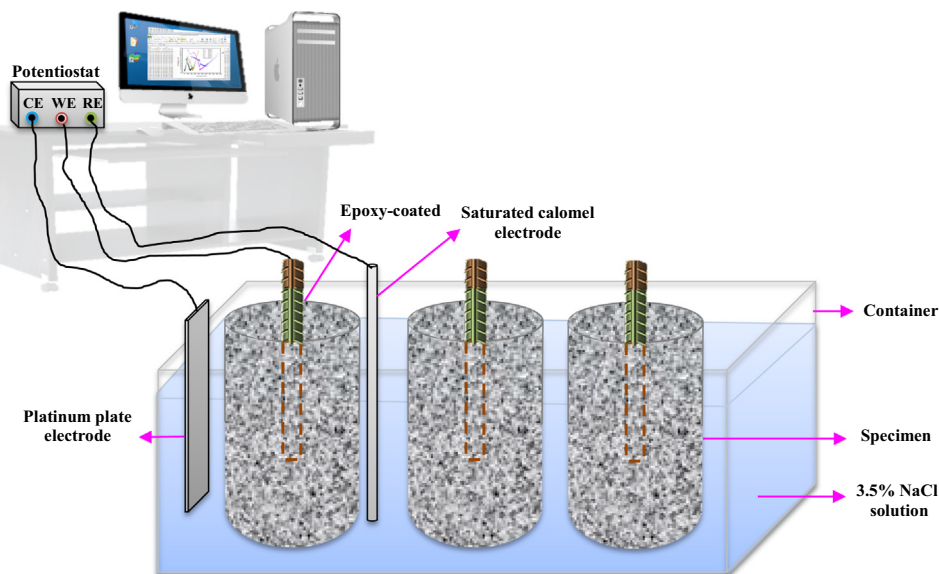


Fig. 2. Experimental setup of the electrochemical tests.

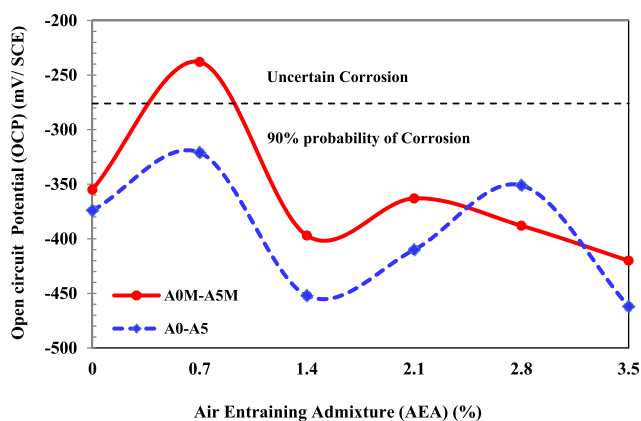


Fig. 3. Open circuit potential (OCP) of all mixes.

AEA dosage increasing from 0 to 0.7%. OCP value decreased (corrosion probability increased) significantly with increasing AEA dosage to 1.4%. This indicates an uncertain corrosion condition (OCP = -218 mV/SCE) for mix A1M containing 0.7% AEA and 10%

MS, whereas all of the remaining mixes had a corrosion probability of more than 90%. These results suggest that the combined use of 0.7% AEA and 10% MS can decrease the corrosion probability of reinforcing bars. However, following ASTM C876 [50], the OCP value should not be interpreted as an indicator of the CR; it can be used to evaluate only the corrosion state of reinforcing bars in concrete. Therefore, other monitoring methods, such as EIS and LPR techniques, were used in the present study to obtain more accurate information about the CR.

4.2. EIS and LPR measurements

Fig. 4 shows a schematic electro-physical model and a typical Nyquist plot of the equivalent electrical circuit used for the reinforcing bar-concrete systems of the present study. In this model (Fig. 4(a)), a parallel circuit of concrete resistivity (R_c) and a constant phase element (CPE_c) at higher frequencies for coated concrete is represented in a series with a parallel circuit of charge transfer resistance (R_{ct}) and a constant phase capacitance element (CPE_{dl}) at lower frequencies for the reinforcing bar surface. Moreover, R_s (i.e., the resistance due to the concrete pore solution) is represented in a series with the two mentioned parallel circuits.

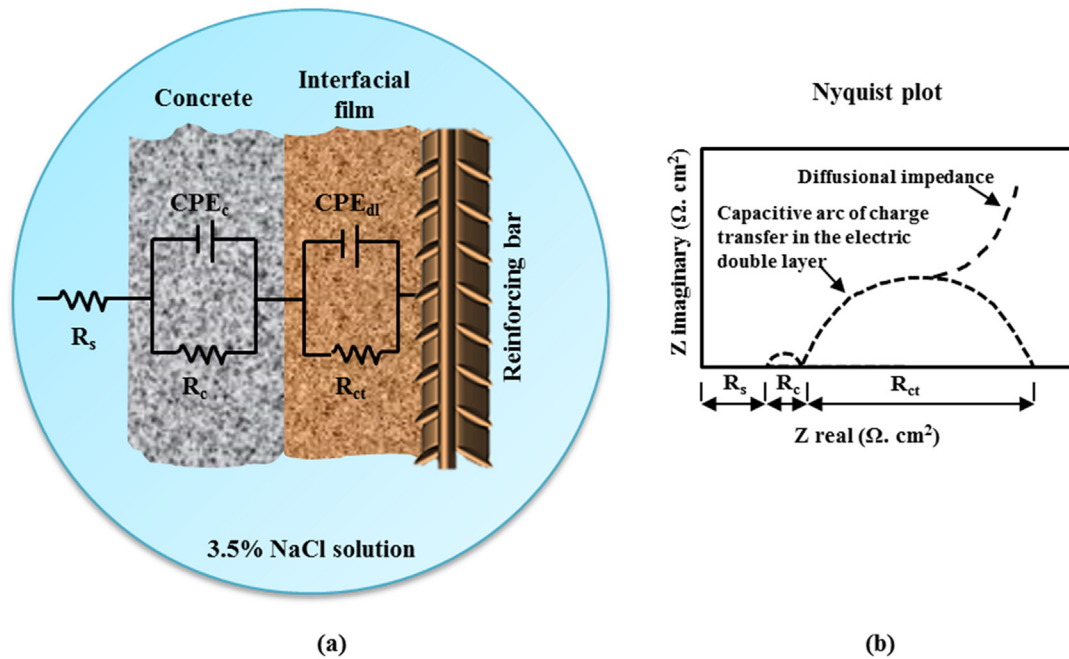


Fig. 4. Schematic representation of (a) the reinforcing bar-concrete interface and (b) a typical Nyquist plot of the equivalent circuit model.

As seen in Fig. 4(b), there are two semi loops in the Nyquist plot. The high-frequency part of the plot relates to the concrete cover of the reinforced concrete, while the low-frequency part is associated with the reinforcing bar surface.

The impedance spectra of all of the mixes were measured, and the results are shown in Figs. 5 and 6 as Nyquist plots considering real (Z') versus imaginary (Z'') impedances. As seen in Fig. 5, although the impedances (both Z' and Z'') of most of the mixes without MS (i.e., A2-A5) were lower than those of the reference mix (A0), the impedance of mix A1 containing 0.7% AEA was the highest among all mixes. It is understood that the impedance indicates the relative permeability of cement-based systems such that the impedance decreases with increasing permeability [63]. Accordingly, it can be concluded that the use of AEA up to a concentration of 0.7% can improve the corrosion resistance of reinforced concrete. This can be attributed to the effect of AEA on reducing concrete bleeding: the air bubbles cause the suspension of the solid particles, which decreases the sedimentation, and, as a result, the water is not expelled. Due to this fact, reduced perme-

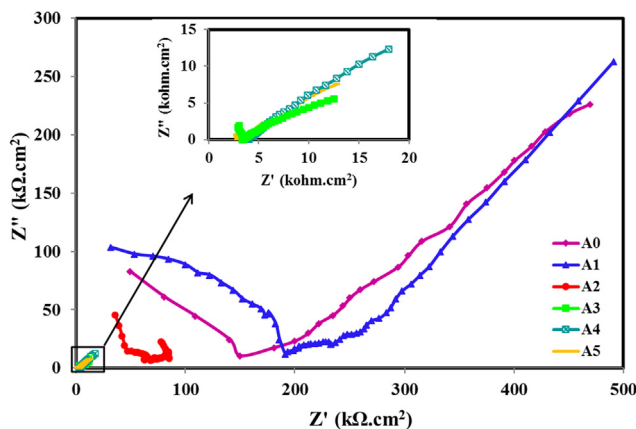


Fig. 5. Nyquist plots for the mixes without MS (A0-A5).

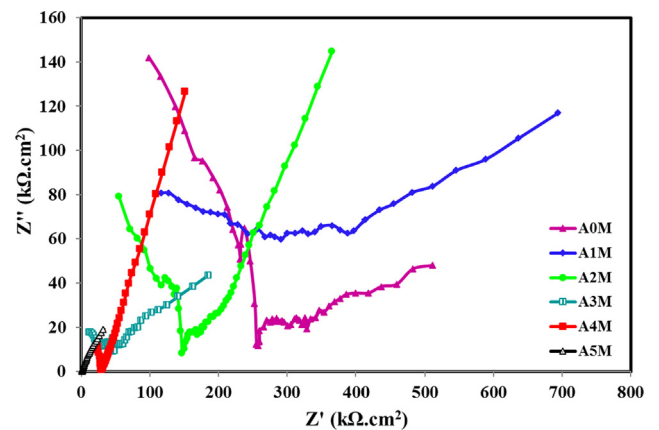


Fig. 6. Nyquist plots for the mixes with MS (A0M-A5M).

ability and the formation of laitance occur, which, in turn, result in improved resistance and durability of reinforced concrete [49].

It can also be seen from Fig. 5 that the addition of higher dosages of AEA (especially doses higher than 1.4%) decreased the impedance. This might have occurred because the high dosage of AEA in the cement mortar provided a network of communicating air bubbles that increase the facility with which water can migrate through the capillary system, resulting in concrete with high absorptivity and permeability properties. This notion has been confirmed by previous studies [14,19], which reported a significant increase in permeability of the mortar of cement-based composites with high AEA dosages.

A similar trend is also evident from Fig. 6 in that the mixes with more than 0.7% AEA exhibited lower impedances than the reference mix (A0). However, it was observed that the impedance of mix A1M containing 0.7% AEA and 10% MS was higher than that of the reference mix (A0). It is also evident from Figs. 5 and 6 that the impedances of the mixes containing MS were higher compared to those of the mixes without MS. This increase at maximum impedance (i.e., mix A1M compared to mix A1) was about 100%,

confirming the effect of MS on decreasing the permeability of such reinforced concrete. This is consistent with the results of previous studies [6,12,64] that reported that MS significantly reduced permeability, thereby enhancing the durability and corrosion resistance of the resulting concrete.

Bode impedance spectra were determined for all of the mixes, and the results are depicted in Figs. 7 and 8. As seen in Fig. 7, the impedances of mixes A2-A5 were within the range of 3 to 22 $k\Omega.cm^2$, whereas the reference mix (A0) had an impedance within the range of 50 to 88 $k\Omega.cm^2$. On the other hand, the impedance of mix A1 containing 0.7% AEA was higher compared to the remaining mixes, and it ranged from 50 to 300 $k\Omega.cm^2$. This, again, confirms the positive effect of AEA (up to 0.7%) on the corrosion resistance of reinforced concrete.

As seen in Fig. 8, the impedance of mix A0M was about three times that of the reference mix (A0), indicating that the use of MS can lead to a noticeable increase in corrosion resistance. The overall trends illustrated in Figs. 7 and 8 are in agreement. Similar findings were also reported in the study by Heniegal et al. [12].

According to the plots of Figs. 5-8, it can be noticed that mix A1M containing 0.7% AEA and 10% MS had an impedance of 380 $k\Omega.cm^2$, which was the highest value among all mixes. This shows that the combination of AEA (up to 0.7%) and MS can provide positive effects on the corrosion resistance of the resulting reinforced concrete members.

Fig. 9 shows the results of the surface porosity of concrete (n_c) and reinforcing bars (n_{dl}) obtained from the EIS test for all of the mixes. The blue and red curves relate to the n_c (left axis) and n_{dl} (right axis) values, respectively. Both of these parameters varied between 0 and 1 such that the values of n_{dl} for most mixes were higher than the n_c values, indicating the role of concrete cover in protecting the reinforcing bar against the penetration of chloride ions. The higher the value of n_c , the more uniform the concrete surface, the closer to the ideal capacitor ($n = 1$) and the lower the expected porosity of the concrete [62]. The closer to 1 the n_{dl} , the more homogeneous the surface; meanwhile, reductions in n_{dl} are associated with increases in the surface roughness, the corrosion of reinforcing bars, and the number of corrosion products formed [65,66].

The results indicate that under optimal conditions, increasing AEA to 0.7% and adding 10% MS (mix A1M) increase n_c by 63% over that of the reference mix (A0). The results also indicate that the maximum values of n_{dl} are associated with the mixes containing 0.7% of AEA (A1 and A1M), reducing the porosity of the reinforcing bar surface by 46% compared to the reference mix (A0). The curves of mixes with MS (A0M-A5M) had a lower fluctuation compared to those of mixes without MS (A0-A5). Moreover, most of the mixes

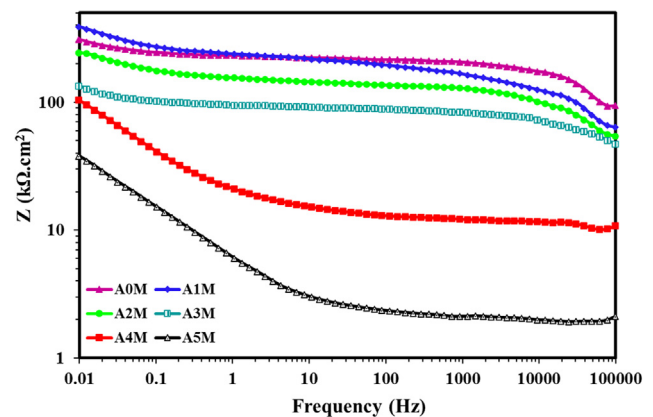


Fig. 8. Bode plot for the mixes with MS (A0M-A5M).

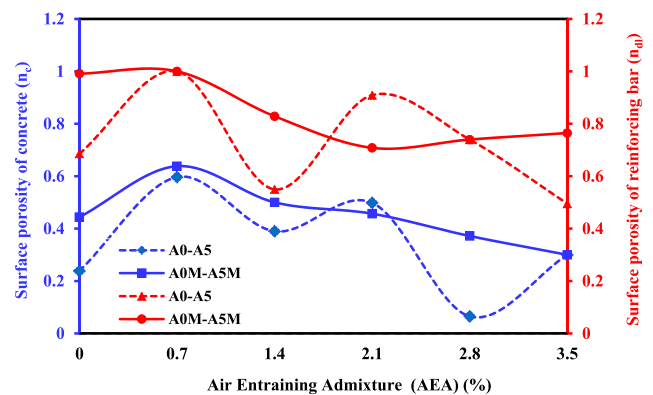


Fig. 9. Comparison between fitted results of n_c and n_{dl} for all mixes.

with MS had higher n_c and n_{dl} values than the mixes without MS, indicating the positive effect of MS on controlling and decreasing the surface porosity of both the concrete and the reinforcing bar.

In order to confirm the mentioned results on the effect of MS and AEA on n_c values, the microstructure of mortars for mixes A0M-A5M was investigated using scanning electron microscopy (SEM) imaging (Fig. 10). The specimens used for SEM imaging were taken from the concrete specimens after electrochemical measurements. After permeating the material's pore system using an epoxy resin, the specimens were cut so that a fresh surface was exposed. Then, the exposed surface was appropriately polished to remove any cutting and grinding damage and to expose an unaltered cross-section of the material's microstructure. It is evident from Fig. 10 that, consistent with the n_c results, mix A1M containing 0.7% AEA and 10% MS had the fewest pores. The finer particles of MS (when compared to cement) and the better interaction of AEA and MS at these dosages were probably the main contributing factors for the observed behavior. However, further increasing the AEA dosage over 0.7% gradually lowers the concrete surface uniformity and increases porosity. As seen in Fig. 10, more and larger pores were evident in mixes A2M-A5M than in mix A1M.

The porosity of the specimens was also measured, and the results are represented in Fig. 11. An experimental equation including the weight of saturated surface dry specimens, dry weight, and the water-immersed weight of specimens was used in calculations as follows:

$$P = \frac{W_{SSD} - W_d}{W_{SSD} - W_w} \times 100\% \quad (3)$$

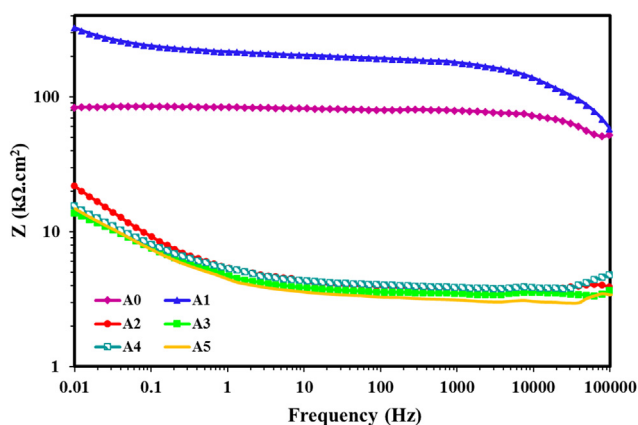


Fig. 7. Bode plot for the mixes without MS (A0-A5).

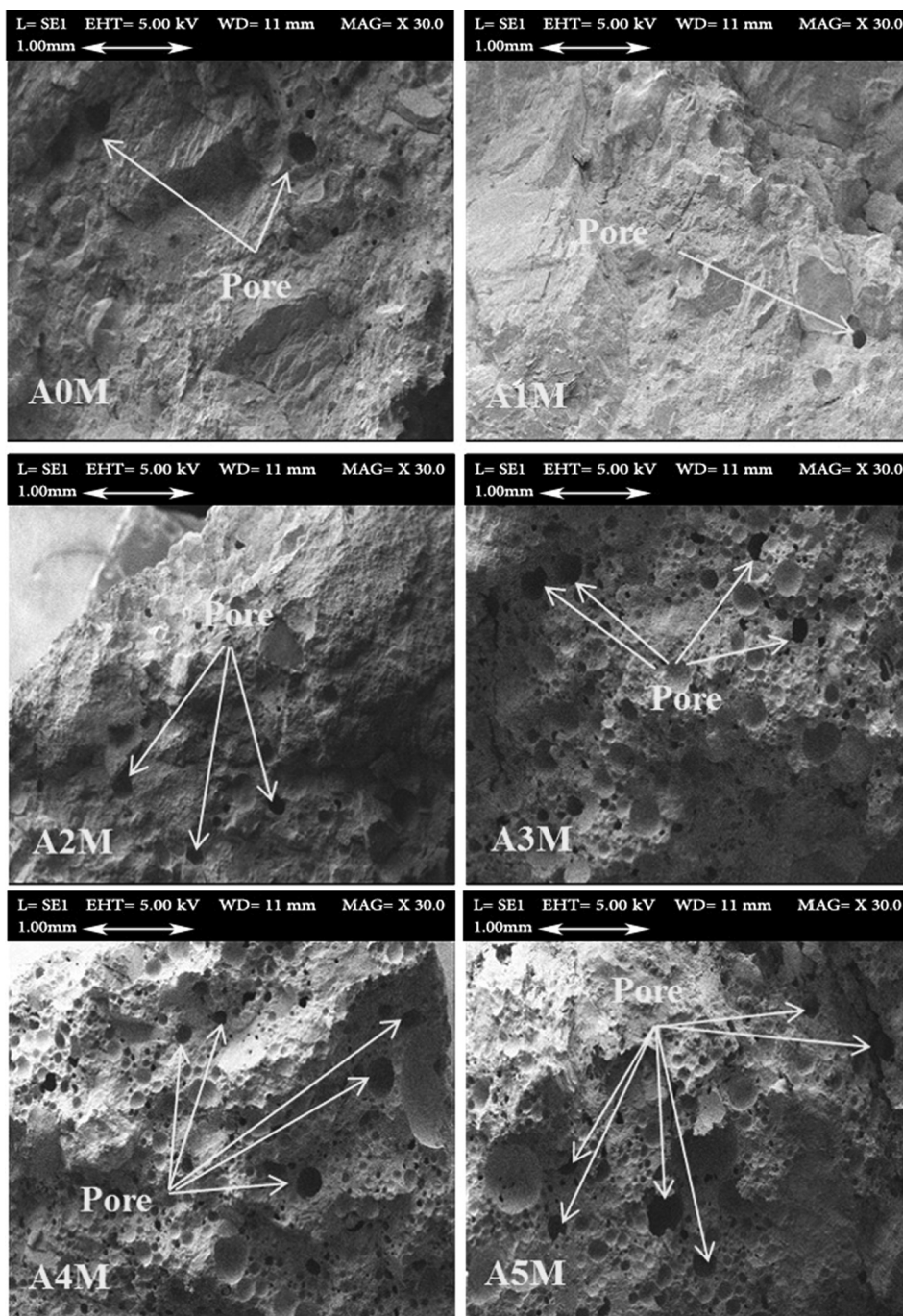


Fig. 10. SEM images of mixes with MS (A0M-A5M).

where P is total porosity (%), W_{SSD} is the weight of saturated surface dry specimens, W_d is the dry weight of the specimens at a temperature of 105 °C, and W_w is the water-immersed weight of the specimens. This is a common method that can successfully measure the porosity of cement-based materials [67–69].

Fig. 11 shows the relationship between total porosity and AEA dosage for all of the mixes. The results indicate that the minimum porosity for both series of mixes with and without MS occurred by using 0.7% AEA. By using more AEA, the total porosity of specimens gradually increased. This was in good agreement with the electrochemical tests and SEM images, showing that using 0.7% AEA with 10% MS is the optimum proportion for obtaining the minimum CR.

In order to characterize the porosity and pore structure distribution of the test specimens, the mercury intrusion porosimetry (MIP) test was conducted on the A1 and A1M mixes, and the results for cumulative and differential pore size are presented in Fig. 12. The A1 and A1M mixes had the optimum corrosion behavior for each series of mixes with and without MS, respectively. The results illustrate that the cumulative pore volume of mix A1M containing 0.7% AEA and 10% MS was lower than mix A1 containing only 0.7% AEA. It can be mentioned that using MS in mix A1M filled the pores and reduced the porosity.

Fig. 13 shows the i_{corr} values obtained from the LPR test for all of the mixes. The A2 mix containing 1.4% AEA was within the range of starting active corrosion, while increasing the AEA dosage gradu-

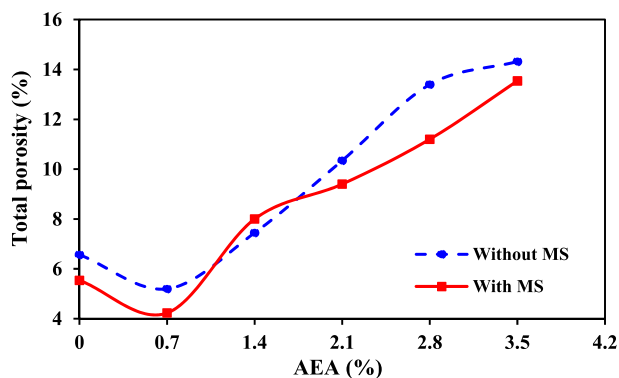


Fig. 11. The total porosity of all mixes.

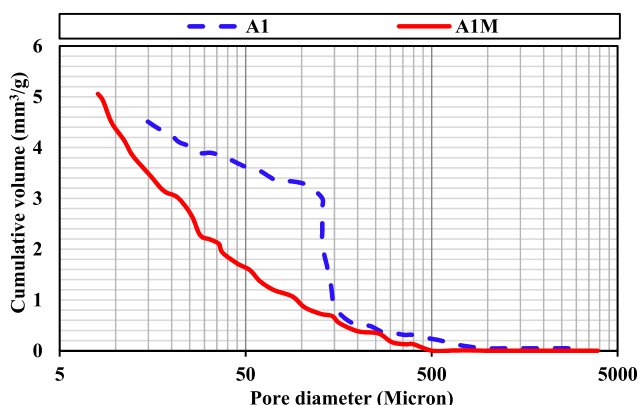


Fig. 12. Representation of pore size distribution for the A1 and A1M mixes.

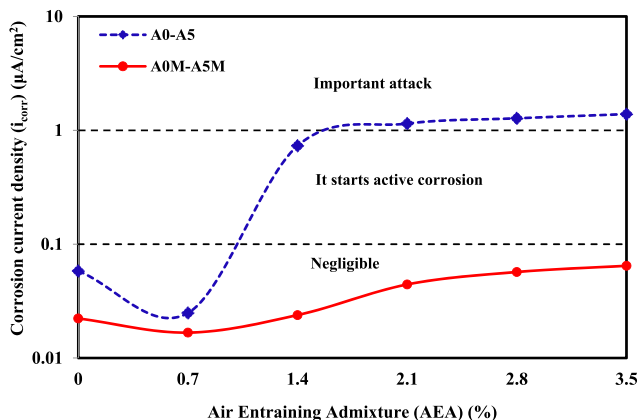


Fig. 13. Changes in the i_{corr} with variations in AEA dosage.

ally increased the i_{corr} and brought it within the range of important attack by chlorides. However, using up to 0.7% AEA decreased the i_{corr} to a negligible corrosion range. This indicates the excellent protection capacity of the A1 mix in relation to the attack by chlorides. As seen in Fig. 11, by adding 10% MS, the i_{corr} values remained within the negligible corrosion range, implying that the chloride ions could not reach the surface of the steel reinforcing bars. The higher corrosion resistance of these mixes may be explained by a delay in the formation of a protective passivation film on the surface of the reinforcing bar [70]. Indeed, the high pozzolanic reactivity and extreme fineness of MS may allow a noticeable decrease in the penetration rate of chlorides [4,7]. As MS is mixed with cement in concrete, it contributes to form calcium silicate hydrate (CSH) as

a result of reacting with free lime during the hydration process. Moreover, MS decreases the volume of large pores and capillaries. As such, a more chemically resistant cement mortar, a denser microscopic pore structure, and a relatively impermeable concrete structure can be achieved.

On the other hand, the addition of MS is expected to reduce the pH of the concrete pore solution (mainly because of the Portlandite consume) [9]. This delays the ingress of chloride in the concrete cover by lowering the chloride threshold for corrosion initiation. Accordingly, the improved electrical resistance and dense microstructure of concrete are expected to be efficient in protecting the reinforcing bar from corrosion in concrete [16].

It is well-known that in chloride-induced corrosion, the stable (self-sustaining) growth of anodic sites requires different conditions, such as a sufficient supply of chloride ions from the surrounding concrete, to be satisfied. Therefore, the repassivation of reinforcing bars may repeatedly occur at the early stages of corrosion initiation. Then, in order to promote active and stable corrosion, further accumulation of chlorides is required. Through the propagation of corrosion, different factors—such as self-healing effects in the case of corrosion in cracked zones, pore filling due to precipitation of corrosion products and other solid phases, and concrete cracking and spalling—might affect the corrosion kinetics [71].

The corrosion kinetics can also be affected by seasonal or other changes in the exposure environment, such as varying moisture conditions. This indicates that with a variation of relative humidity (RH), different volume fractions of the pore system of concrete are filled with water. When RH is in the range of low to intermediate, a considerable tension may be applied to the pore liquid in small pores at the concrete-reinforcing bar interface, causing them not to be able to behave as a liquid. On the other hand, when RH is high (i.e., RH greater than 80%), the tension decreases to a level approaching bulk solution behavior. Meanwhile, with an increase of RH, the radius of stably water-filled pores effectively increases in a non-linear manner. Accordingly, the surface area of the reinforcing bar, which is in contact with liquid water and capable of behaving as an electrolyte, can be expected to increase non-linearly with RH [72]. As a consequence, the water-filled porosity is increased. In turn, losses in the reinforcing bar sectional area or corrosion-induced cracking of the concrete may occur, thereby influencing the structural integrity and load-bearing capacity—and, thus, the safety—of reinforced concrete.

In the current study, according to the SEM and LPR results, incorporating 0.7% AEA and 10% MS decreased the pore structure and appropriately affected the corrosion kinetics. By clogging the available pores and reducing the RH, this effectively decreased the CR.

Fig. 14 shows the variations of R_c and R_{ct} (from the EIS test), as well as R_p and CR (from the LPR test) for different mixes. The blue and red curves in Fig. 14(a) are related to the R_c and R_{ct} , respectively. Meanwhile, in Fig. 14(b), they are related to the R_p and CR, respectively. Fig. 14(a) shows that the highest values of R_c and R_{ct} corresponded to the A1M mix containing 0.7% AEA and 10% MS. For the other mixes, these values were much closer to 0.

Considering the Stern-Geary equation and a value of 26 mV for the B constant, the corrosion level was considered very high when R_p was $<26 \text{ k}\Omega\cdot\text{cm}^2$, high in the range between 26 and 52 $\text{k}\Omega\cdot\text{cm}^2$, low to moderate in the range between 52 and 260 $\text{k}\Omega\cdot\text{cm}^2$, and negligible for polarization resistance values greater than 260 $\text{k}\Omega\cdot\text{cm}^2$. As seen in Fig. 14(b), among the mixes with AEA and without MS (A1-A5), mix A1 was in the negligible corrosion level, mix A2 was in the high corrosion level, and mixes A3-A5 had R_p values in the very high corrosion level. This indicates that the increase in AEA up to 0.7% increases the R_p to more than 2.3 times the reference mix (A0), positively affecting the corrosion behavior of

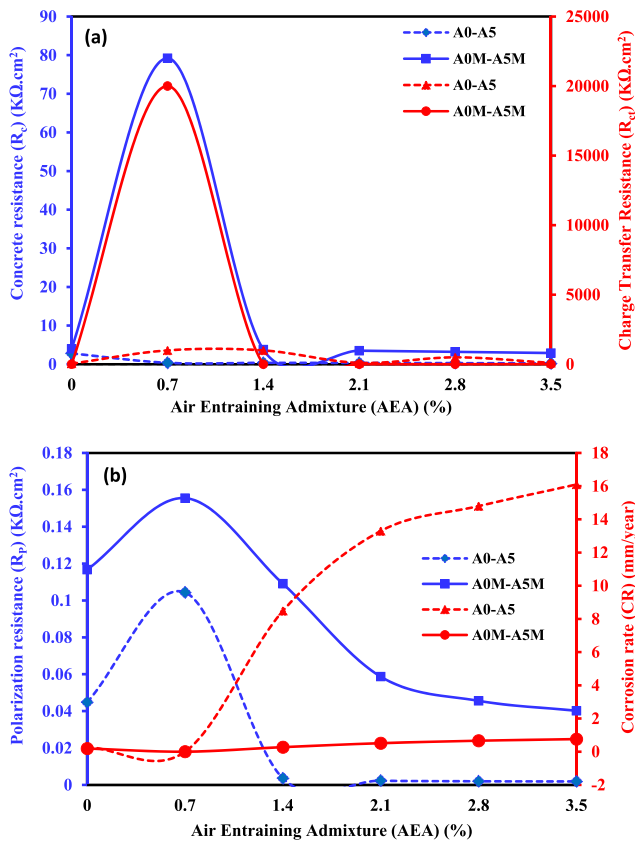


Fig. 14. Fitted data of R_c , R_{ct} , R_p and CR for all mixes.

reinforced concrete. As seen in Fig. 14(b), the R_p values of the mixes with MS were 1.33 to 1.97 times higher than those of the mixes without MS. A similar trend was observed for the CR values: the mixes with MS had CRs that were 1 to 31 times lower than the mixes without MS. It can be implied that adding MS as a cement replacement (here, 10%) can enhance the corrosion properties of reinforced concrete. This higher corrosion resistance of reinforcing bars (which is due to the micro-filler action and enhanced bonding capability of the MS particles) may be associated with the improved microstructure of cement mortar. According to Fig. 14, mix A1M containing 0.7% AEA and 10% MS included the highest R_c , R_{ct} , and R_p and the lowest CR. At up to 0.7% AEA, the air bubbles that developed were well-distributed without a connection between them. They may interrupt the capillary channels near the surface, thereby preventing the penetration of water. This was also confirmed in the study by Mendes et al. [19]. Accordingly, it can be concluded that the addition of 10% MS to the mix containing up to 0.7% AEA can provide improved performance of these two admixtures (AEA and MS) in cement mortar, resulting in a considerable protection capacity against chloride attack for the final reinforced concrete.

4.3. Mechanism of AEA and MS interaction

In order to better illustrate the role of AEA (air bubbles) and MS in mix A1M containing 0.7% AEA and 10% MS, the mechanism of their interactions in concrete mixes is schematically shown in Fig. 15. As seen in Fig. 15(a), there were some interactions at solid-water-air interfaces. At the air-water interface, the polar groups of air bubbles are oriented towards the water phase. Simultaneously, at the solid-water phase, the polar groups are absorbed into the cement, whereas the non-polar groups are oriented to the

water phase. This makes the cement surface hydrophobic; hence, the water can be displaced by air bubbles, which remain linked to the cement particles. At this stage, as seen in Fig. 15(b), the air bubbles in the mix are dispersed with the help of a mass of cement particles, decreasing the tendency of air bubbles to float to the surface. On the other hand, the rate of settlement of cement particles may be reduced by the flotation force of the air bubbles. This mechanism, together with the micro-filling activity of the MS particles and the role of some separate air bubbles in interrupting the capillary channels, decreases the tendency of bleeding and segregation, as well as water penetration in the concrete mix.

5. Comparison of the present study with previous studies

A comparison study was also conducted to better place the findings of the current study within the existing literature. Specifically, mix A1M, as the optimal mix of the present study, was selected for comparison with mixes examined in previous studies. Comparisons were made in terms of impedance (i.e., Nyquist and Bode plots), R_p , CR, n_c , and n_{dl} . Table 5 summarizes the main parameters considered in previous studies on the topic.

Four of the reviewed studies [9,64,73,76] that reported the impedance using Nyquist plots are compared with mix A1M in Fig. 16. The impedances of the mix containing 30% MS and 30% FA as a cement replacement [73](a) were higher than those of the mixes containing 7.5% MS [64] and 50% NS [73](b). Also, exposing concrete mixes containing different mineral admixtures to a chloride solution for 154 days (22 cycles of attack) showed that the impedance of the mix containing 10% MS [9](a) was higher than that of mixes containing 25% FA [9](b) and 30% MK [9](c). This can be explained by the improved resistance to chloride penetration because of the lower amounts of capillarity and absorbed water for the mix containing MS [9](a) compared to those of the mixes containing FA [9](b) and MK [9](b). Accordingly, in the mixes [9](a, b and c) [73](a and b) that utilized different admixtures, using MS resulted in a more effective improvement in impedance compared to using other admixtures. Among whole impedances, the minimum value was reported for the study that used 5% of an inhibitor [76], whereas the maximum one was associated with the optimal mix of the present study (A1M) containing 0.7% AEA and 10% MS. The difference observed between the impedances of mix A1M and those of other reviewed mixes may be attributed to the combined effect of 0.7% AEA and 10% MS on increasing the corrosion resistance of concrete [82].

A comparison between the reported values of R_p and the CR of mix A1M with the existing studies [9,64,70,74–76,78–81] is represented in Fig. 17. As seen in Fig. 17(a), similar to mix A1M, different mixes of [9](a, b and c) and [74](a and b) had a negligible corrosion level (R_p greater than 260 $k\Omega \cdot cm^2$), the mixes of [64,75,79] had a low to moderate corrosion level ($52 < R_p < 260 k\Omega \cdot cm^2$), the mixes of [78](a and b) and [80] had a high corrosion level ($26 < R_p < 52 k\Omega \cdot cm^2$), and the mixes of [70](a, b, and c) and [78](c) had a very high corrosion level ($R_p < 26 k\Omega \cdot cm^2$). As seen in Fig. 17(b), according to the ranges mentioned in the study by Fodil and Mohamed [78], only mix A1M was in the negligible corrosion level ($CR < 0.001 mm/year$), while the mixes of [76] and [78](b) were in the low corrosion level ($0.001 < CR < 0.005 mm/year$), the mixes of [81] and [78](a) were in the moderate corrosion level ($0.005 < CR < 0.01 mm/year$), and other mixes, including the mixes of [64,70], and [78](c), were in the high corrosion level.

From Fig. 17(a), it can be mentioned that the use of HDPE and PP is more effective in improving the corrosion level than the use of perlite as a partial replacement of conventional aggregates [78](a). Similarly, the use of MK [17](a) and FA [17](b) is more influential than NP [78](b and c) as a partial replacement of cement.

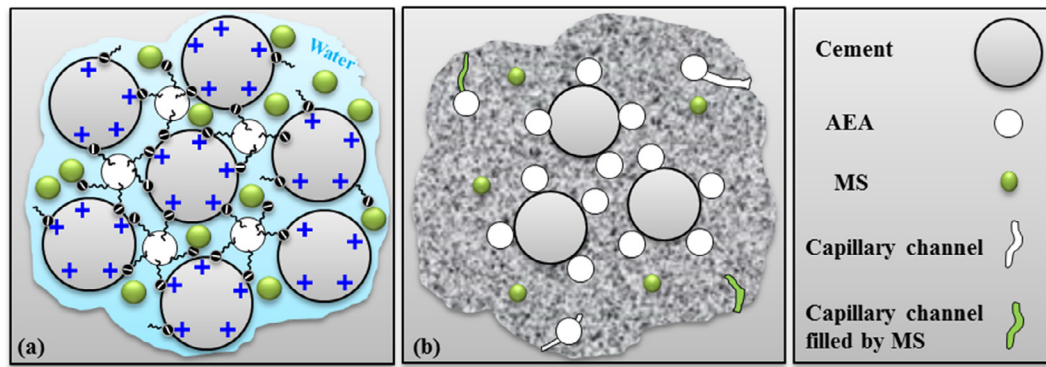


Fig. 15. A schematic view of the mechanism of (a) first and (b) second states of AEA and MS interactions in mix A1M containing 0.7% AEA and 10% MS.

Table 5
Summary of different parameters considered in existing studies.

Reference (mix)	Type and dosage of admixture	Cement strength class (MPa)	Type of reinforcing bar	Inhibitor	Type of aggregates	Exposure
A1M	0.7% AEA + 10% MS	52.5	Steel	-	-	3.5% NaCl
[9](a)	10% MS	32.5	Carbon steel	-	-	5% NaCl
[9](b)	25% Fly Ash (FA)	32.5	Carbon steel	-	-	5% NaCl
[9](c)	30% Metakaolin (MK)	32.5	Carbon steel	-	-	5% NaCl
[62]	10% Marble and Granite waste dust (MGWD)	-	Steel	-	-	3.5% NaCl
[64]	7.5% MS	-	Steel	-	-	5% NaCl
[70](a)	27% MS + 3% Nano silica (NS)	52.5	Steel	-	-	5% NaCl
[70](b)	27% MS	52.5	Steel	-	-	5% NaCl
[70](c)	25% MS	52.5	Steel	-	-	5% NaCl
[73](a)	30% MS + 30% FA	52.5	Steel	-	-	Carbonation
[73](b)	50% NS	42.5	Steel	-	-	Carbonation
[74](a)	-	-	Steel	-	12% High density polyethylene (HDPE)	5% NaCl
[74](b)	-	-	Steel	-	12% Polypropylene (PP)	5% NaCl
[75]	-	42.5	Low-alloy reinforcing steel (LA)	-	-	3.5% NaCl
[76]	-	-	Steel	5%	-	3.5% NaCl
[77]	-	52.5	Steel fiber	-	-	2% NaCl
[78](a)	-	42.5	Steel	-	10% Perlite	5% NaCl
[78](b)	10% Natural pozzolan (NP)	42.5	Steel	-	-	5% NaCl
[78](c)	30% NP	42.5	Steel	-	-	5% NaCl
[79]	-	-	Steel	-	-	0.8 Molar NaOH
[80]	-	-	Steel	50%	-	3.5% NaCl
[81]	11% MS	-	Steel	-	-	3% NaCl

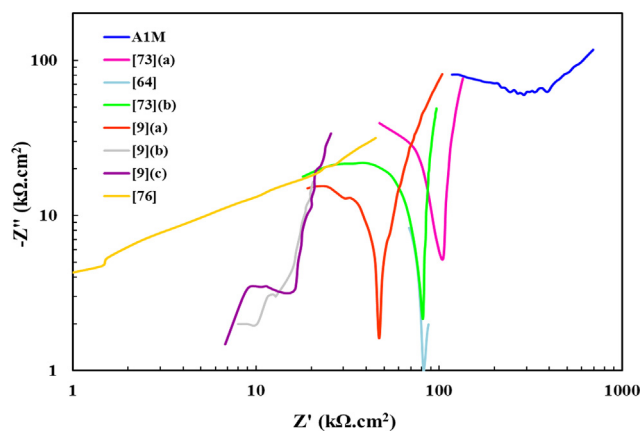


Fig. 16. Comparison of the Nyquist plot of mix A1M with the existing studies.

Considering the values of R_p and the CR, it can be noted that the performance of a low concentration of inhibitor [76] is generally

better than a high concentration [80] in order to achieve the required inhibition of reinforcing bar corrosion. Furthermore, the results for the mixes with MS indicate that the mix [9](a) that utilized 10% MS had an improved corrosion behavior over other mixes [70](a, b, and c) that used more than 25% MS. On the other hand, the results of R_p and the CR were inversely reported for the corrosion level of the mix [64] that utilized 7.5% MS. In this way, Khedr and Idriss [25] evaluated the effectiveness of MS in concrete subjected to corrosion damage of the embedded reinforcing bar. MS dosages of 0, 10, 15, 20, and 25% were used as partial replacements of ordinary Portland cement. Their results indicate that an optimal effect is observed in the range of 10–15% MS replacement dosage while at higher dosages of MS (i.e., 20–25%), the corrosion resistance of concrete is noticeably decreased. This is also confirmed by the results observed for mix A1M, including the highest R_p and the lowest CR among whole mixes of the evaluated existing studies. The combined effect of 0.7% AEA and 10% MS on the micro-structure of mix A1M may be the reason for these improved corrosion properties.

The reported values of n_c and n_{dl} for the mixes of three studies [62,74,77] are represented in Fig. 18 in comparison with the values

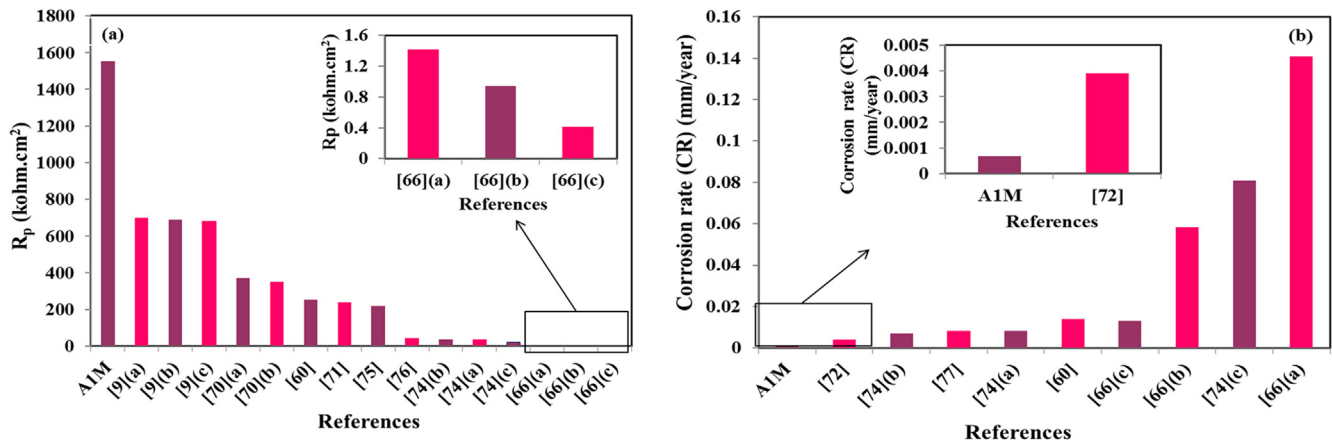


Fig. 17. Comparison of the R_p and CR values of mix A1M with the existing studies.

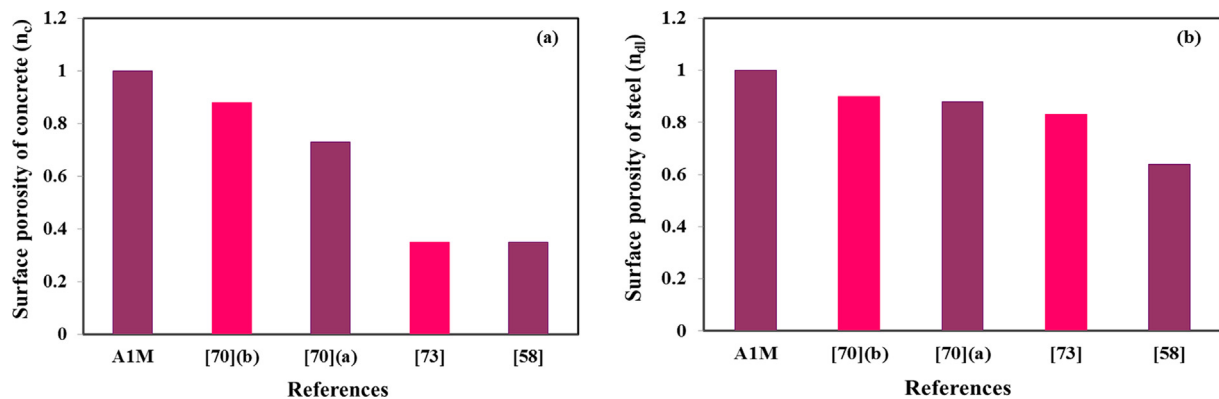


Fig. 18. Comparison of the n_c and n_{di} values of mix A1M with the existing studies.

of mix A1M provided in the present study. As mentioned, the closer to 1 the n_c and n_{di} are, the lower the surface porosity of the concrete and the reinforcing bar, respectively. Accordingly, the results in Fig. 18 indicate that replacing the conventional aggregate by 12% HDPE [74](b) can retain the n_c and n_{di} closer to 1 than by replacing by 12% PP [74](a). On the other hand, the use of these thermoplastic polymers (i.e., HDPE and PP) is more influential than the use of steel fiber [77] and MGWD [62] in improving the surface porosity of both the concrete and the reinforcing bar. However, in the present study, mix A1M had the lowest surface porosity among all mixes, as it had the highest n_c and n_{di} values. This, again, confirms the positive interaction of 0.7% AEA and 10% MS to improve the reinforced concrete properties against penetration attacks.

6. Statistical analysis

6.1. Extreme vertices mixture analysis

The present study implemented the extreme vertices mixture analysis in Minitab[®]-18 [83]. This method is used for laboratory data analysis, sensitivity analysis, and mix component optimization, including AEA (X_1) and MS (X_2). The ranges of these components were $0 \leq X_1 \leq 3.6\%$ and $0 \leq X_2 \leq 10\%$. The responses considered for determining the optimal values included Y_1 (R_c), Y_2 (R_{ct}), Y_3 (R_p), and Y_4 (CR).

6.1.1. Response trace plot

The response trace plot assesses the effect of change in each particular mix component on the targeted response. Fig. 19 shows

the effects of AEA and MS, as well as the sensitivity of the responses, including R_c , R_{ct} , R_p , and CR to each of these components. It can be seen that with an increase in both AEA and MS dosages, the values of R_c , R_{ct} , and R_p increase, while the value of CR decreases. However, the plots of whole responses represent a little reverse effect at their later stage. Moreover, based on the steeper slopes of mix components (AEA and MS) in the plots of R_c and R_{ct} rather than R_p and CR, it can be stated that the values of R_c and R_{ct} are more sensitive to changes in AEA and MS compared to the values of R_p and CR.

6.1.2. Optimization of the responses

In the present study, the response optimization was also conducted to obtain the optimal dosages of AEA and MS for different responses (i.e., R_c , R_{ct} , R_p , and CR). Response optimization determines the combined settings of input variables that simultaneously optimize a single response or set of responses. The plots of predicted optimal dosages of AEA and MS for the maximum R_c , R_{ct} , and R_p and the minimum CR are depicted in Fig. 20. In the figure, y represents the optimal response, and d represents the composite desirability (in a range of 0–1) as a measure of how the combined goals for all of the responses are satisfied by the represented solution. A composite desirability equal to zero indicates that one or more responses are outside of their acceptable limits, while one denotes the ideal case. As seen in Fig. 20, the optimal responses were achieved for the dosages of AEA and MS in the ranges of 0.6 to 0.69% and 9.31 to 9.4%, respectively, with an acceptable mean desirability of prediction for all responses.

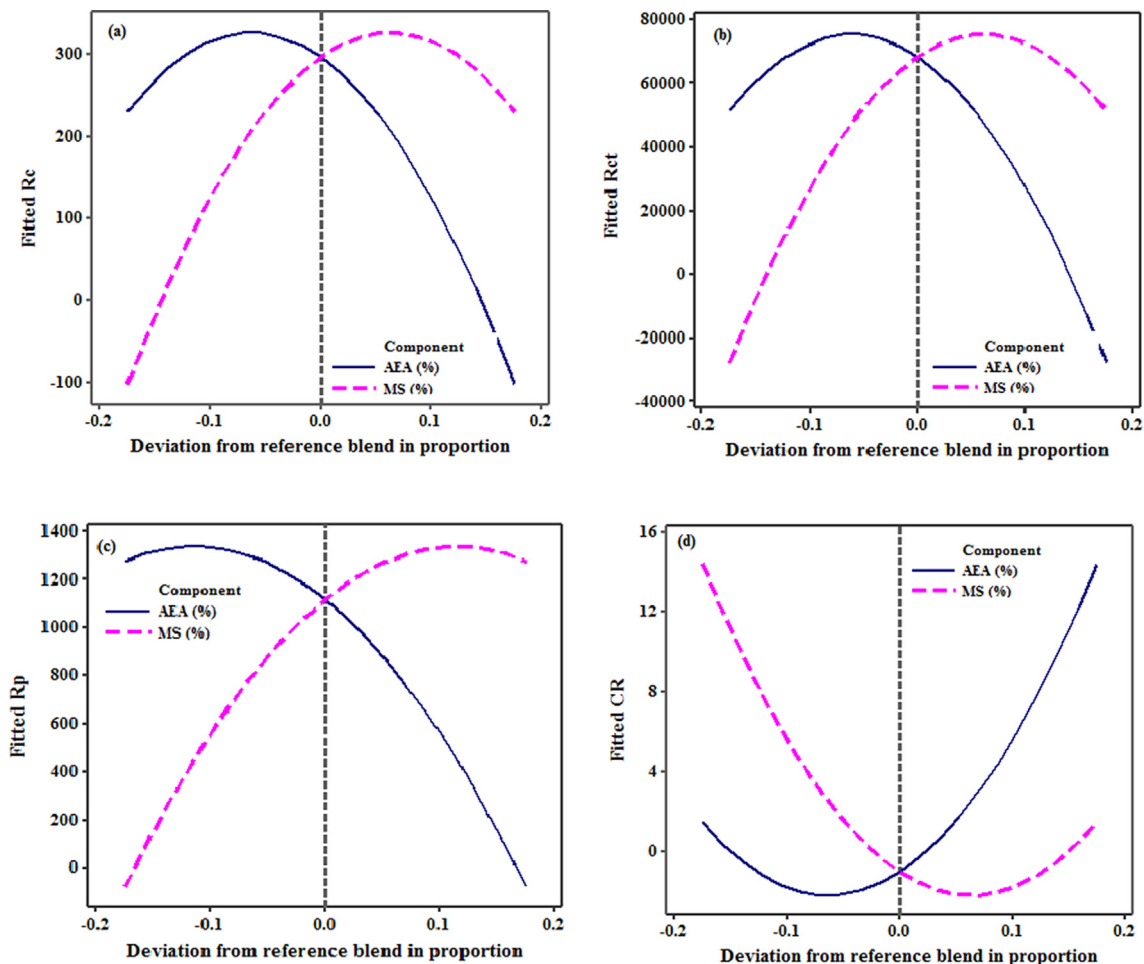


Fig. 19. Cox response trace plots for the R_c (a), R_{ct} (b), R_p (c) and CR (d).

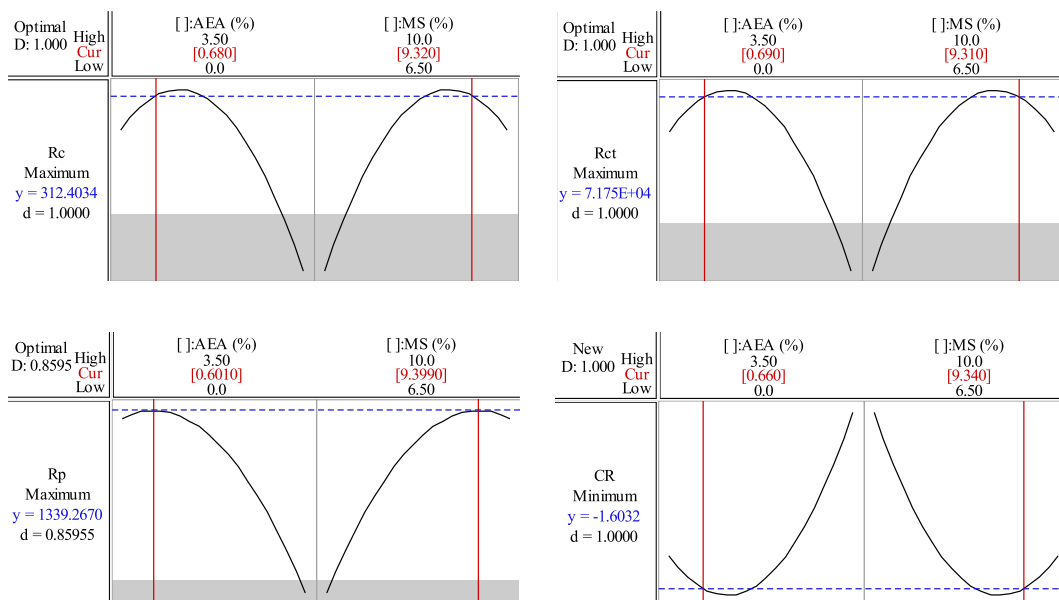


Fig. 20. Response optimization plots showing the optimal values of mix components for the optimal R_c , R_{ct} , R_p , and CR.

Table 6
Results of the ANOVA for R_c .

Percent of Contribution (PC)	F statistic	Mean square (MS)	Sum of square (SS)	Degree of freedom (DF)	Source
43	0.98	473	2365	5	AEA (%)
13	1.46	708	708	1	MS (%)
44	–	483	2417	5	Error
100	–	–	5491	11	Total

Table 7
Results of the ANOVA for R_{ct} .

Percent of Contribution (PC)	F statistic	Mean square (MS)	Sum of square (SS)	Degree of freedom (DF)	Source
49.5	1.14	35,591,200	177,955,998	5	AEA (%)
7	0.80	24,862,632	24,862,632	1	MS (%)
43.5	–	31,254,171	156,270,855	5	Error
100	–	–	359,089,486	11	Total

Table 8
Results of the ANOVA for R_p .

Percent of Contribution (PC)	F statistic	Mean square (MS)	Sum of square (SS)	Degree of freedom (DF)	Source
58.5	11.8	359,322	1,796,611	5	AEA (%)
36.5	36.9	1,121,185	1,121,185	1	MS (%)
5	–	30,362	151,809	5	Error
100	–	–	3,069,605	11	Total

Table 9
Results of the ANOVA for CR.

Percent of Contribution (PC)	F statistic	Mean square (MS)	Sum of square (SS)	Degree of freedom (DF)	Source
29.6	1.17	28	139	5	AEA (%)
45	8.88	213	213	1	MS (%)
25.4	–	24	120	5	Error
100	–	–	473	11	Total

6.2. The analysis of variance (ANOVA)

The analysis of variance (ANOVA) as a statistical method is mainly used to determine the percent of contribution (PC) of each parameter to the results [84,85]. In this study, the ANOVA analysis was conducted using Minitab®-18 [83] to determine the effective parameters on R_c , R_{ct} , R_p , and CR, and the results are presented in Tables 6–9, respectively. The ANOVA shows that the contribution of AEA in improving the R_c (PC = 43%), R_{ct} (PC = 49.5%) and R_p (PC = 58.5%) of the mixes was higher than that of MS (PC = 13%, 7% and 36.5% for R_c , R_{ct} and R_p , respectively). However, this trend was reversed for the CR, for which MS (PC = 45%) was a more influential factor than AEA (PC = 29.6%).

7. Conclusions

In this study, the effect of incorporating air-entraining admixture (AEA) and micro-silica (MS) as partial replacements of cement on the corrosion behavior of reinforced concrete was evaluated, and the following conclusions were drawn:

1. OCP measurements indicate that all the mixes without MS have corrosion potentials more negative than -276 mV/SCE, indicating that their corrosion probability is more than 90%. On the other hand, for the mixes with MS, there is a significant increase in OCP value (decrease in corrosion probability), with AEA dosage increasing from zero to 0.7%. Then, the OCP value

decreases (corrosion probability increases) significantly as the AEA dosage increases to 1.4%. This indicates an uncertain corrosion condition (OCP = -218 mV/SCE) for mix A1M containing 0.7% AEA and 10% MS, whereas all the remaining mixes have a corrosion probability of more than 90%.

2. EIS measurements reveal that using up to 0.7% AEA as a cement replacement increases the impedance, maximum concrete resistance against penetration (R_c) and electrical charge transfer resistance of the reinforcing bar (R_{ct}), as well as decreases the surface porosity of the concrete (n_c) and the reinforcing bar (n_{dl}). However, at higher dosages of AEA, the reversed values of these parameters are observed due to the formation of a network of communicating air bubbles that increase the facility with which water can migrate through the capillary system, resulting in concrete with high absorptivity and permeability properties. Furthermore, the addition of 10% MS as a cement replacement, because of providing a denser microstructure in mortar, improves these parameters and, thus, the corrosion resistance of reinforced concrete.
3. LPR measurements reveal that using up to 0.7% AEA keeps the corrosion current density (i_{corr}) in a negligible corrosion range, whereas an additional increase in the AEA dosage gradually moves the i_{corr} to the range of starting active corrosion and then, to the range of significant attacks by chlorides. Moreover, by adding 10% MS, the i_{corr} values of whole mixes remain within the negligible corrosion range, implying that the chloride ions could not reach the surface of the steel reinforcing bars.

4. LPR measurements also reveal that the polarization resistance (R_p) and corrosion rate (CR) values of the mixes with MS as a cement replacement (here, 10%) are 1.33 to 1.97 times higher and 1 to 31 times lower than those of the mixes without MS, respectively. It can be implied that adding MS as a cement replacement (here, 10%) can enhance the corrosion properties of reinforced concrete due to the micro-filler action and enhanced bonding capability of the MS particles.
5. The results of comparing the present study with existing studies indicate that the most improved corrosion behavior, among whole mixes, corresponds to the optimal mix of the present study containing 0.7% AEA and 10% MS as a cement replacement.
6. The statistical analysis reveals that optimal responses are achieved for the dosages of AEA and MS in the ranges of 0.6 to 0.69% and 9.31 to 9.4%, respectively. Also, the AEA dosage is a more influential factor in improving the R_c , R_{ct} , and R_p , whereas the MS dosage is a more influential factor in reducing the CR.

The promising findings of the current study contribute toward a better understanding of the combined effect of AEA and MS on the structure of cement mortar. The optimal data obtained in this study, together with the available data in the literature, have the potential to meaningfully improve the corrosion behavior of reinforced concrete by incorporating AEA and MS as a partial replacement of cement.

CRedit authorship contribution statement

Anis Ghanei: Investigation, Writing - original draft, Methodology. **Hamid Eskandari-Naddaf:** Project administration, Supervision, Conceptualization, Writing - review & editing, Methodology. **Togay Ozbakkaloglu:** Writing - review & editing, Validation. **Ali Davoodi:** Conceptualization.

Declaration of Competing Interest

The authors declare that they have no known competing financial interests or personal relationships that could have appeared to influence the work reported in this paper.

Acknowledgment

The authors appreciate the support for this investigation by the central laboratory of Hakim Sabzevari University (a member of the network of Iranian science laboratories-NISL).

References

- [1] M. Azimi-Pour, H. Eskandari-Naddaf, ANN and GEP prediction for simultaneous effect of nano and micro silica on the compressive and flexural strength of cement mortar, *Constr. Build. Mater.* 189 (2018) 978–992.
- [2] H. Eskandari-Naddaf, A. Ziaei-Nia, Simultaneous effect of nano and micro silica on corrosion behaviour of reinforcement in concrete containing cement strength grade of C-525, *Procedia Manuf.* 22 (2018) 399–405.
- [3] S.A. Emamian, H. Eskandari-Naddaf, Effect of porosity on predicting compressive and flexural strength of cement mortar containing micro and nano-silica by ANN and GEP, *Constr. Build. Mater.* 218 (2019) 8–27.
- [4] A. Kooshkaki, H. Eskandari-Naddaf, Effect of porosity on predicting compressive and flexural strength of cement mortar containing micro and nano-silica by multi-objective ANN modeling, *Constr. Build. Mater.* 212 (2019) 176–191.
- [5] L.G. Li, Z.H. Huang, J. Zhu, A.K.H. Kwan, H.Y. Chen, Synergistic effects of micro-silica and nano-silica on strength and microstructure of mortar, *Constr. Build. Mater.* 140 (2017) 229–238.
- [6] L.G. Li, J. Zhu, Z.H. Huang, A.K.H. Kwan, L.J. Li, Combined effects of micro-silica and nano-silica on durability of mortar, *Constr. Build. Mater.* 157 (2017) 337–347.
- [7] W. Wu, R. Wang, C. Zhu, Q. Meng, The effect of fly ash and silica fume on mechanical properties and durability of coral aggregate concrete, *Constr. Build. Mater.* 185 (2018) 69–78.
- [8] P.K. Mehta, O.E. Gjorv, Properties of portland cement concrete containing fly ash and condensed silica-fume, *Cem. Concr. Res.* 12 (5) (1982) 587–595.
- [9] A.M.d. Oliveira, O. Cascudo, Effect of mineral additions incorporated in concrete on thermodynamic and kinetic parameters of chloride-induced reinforcement corrosion, *Constr. Build. Mater.* 192 (2018) 467–477.
- [10] A. Madadi, H. Eskandari-Naddaf, R. Shadnia, L. Zhang, Digital image correlation to characterize the flexural behavior of lightweight ferrocement slab panels, *Constr. Build. Mater.* 189 (2018) 967–977.
- [11] M. Manera, Ø. Vennesland, L. Bertolini, Chloride threshold for rebar corrosion in concrete with addition of silica fume, *Corros. Sci.* 50 (2) (2008) 554–560.
- [12] A.M. Heniegal, M. Amin, H. Youssef, Effect of silica fume and steel slag coarse aggregate on the corrosion resistance of steel bars, *Constr. Build. Mater.* 155 (2017) 846–851.
- [13] M.I. Khan, R. Siddique, Utilization of silica fume in concrete: Review of durability properties, *Resour. Conserv. Recycl.* 57 (2011) 30–35.
- [14] P. Choi, J.H. Yeon, K.-K. Yun, Air-void structure, strength, and permeability of wet-mix shotcrete before and after shotcreting operation: The influences of silica fume and air-entraining agent, *Cem. Concr. Compos.* 70 (2016) 69–77.
- [15] A. Farahani, H. Taghaddos, M. Shekarchi, Prediction of long-term chloride diffusion in silica fume concrete in a marine environment, *Cem. Concr. Compos.* 59 (2015) 10–17.
- [16] J.M.R. Dotto, A.G.d. Abreu, D.C.C. Dal Molin, I.L. Müller, Influence of silica fume addition on concretes physical properties and on corrosion behaviour of reinforcement bars, *Cem. Concr. Compos.* 26 (1) (2004) 31–39.
- [17] Y.e. Qing, Z. Zenan, K. Deyu, C. Rongshen, Influence of nano-SiO₂ addition on properties of hardened cement paste as compared with silica fume, *Constr. Build. Mater.* 21 (3) (2007) 539–545.
- [18] P. Van den Heede, J. Furniere, N. De Belie, Influence of air entraining agents on deicing salt scaling resistance and transport properties of high-volume fly ash concrete, *Cem. Concr. Compos.* 37 (2013) 293–303.
- [19] J.C. Mendes, T.K. Moro, A.S. Figueiredo, K.D.d.C. Silva, G.C. Silva, G.J.B. Silva, R.A. F. Peixoto, Mechanical, rheological and morphological analysis of cement-based composites with a new LAS-based air entraining agent, *Constr. Build. Mater.* 145 (2017) 648–661.
- [20] C.-W. Chung, C.-S. Shon, Y.-S. Kim, Chloride ion diffusivity of fly ash and silica fume concretes exposed to freeze–thaw cycles, *Constr. Build. Mater.* 24 (9) (2010) 1739–1745.
- [21] A. Ziaei-Nia, G.-R. Tadayonfar, H. Eskandari-Naddaf, Effect of Air Entraining Admixture on Concrete under Temperature Changes in Freeze and Thaw Cycles, *Mater. Today: Proc.* 5 (2) (2018) 6208–6216.
- [22] M.P. Kumar, K.M. Mini, M. Rangarajan, Ultrafine GGBS and calcium nitrate as concrete admixtures for improved mechanical properties and corrosion resistance, *Constr. Build. Mater.* 182 (2018) 249–257.
- [23] A.S. Castela, B.S. da Fonseca, R.G. Duarte, R. Neves, M.F. Montemor, Influence of Unsupported Concrete Media in Corrosion Assessment for Steel Reinforcing Concrete by Electrochemical Impedance Spectroscopy, *Electrochim. Acta* 124 (2014) 52–60.
- [24] B. Assouli, F. Simescu, G. Debicki, H. Idrissi, Detection and identification of concrete cracking during corrosion of reinforced concrete by acoustic emission coupled to the electrochemical techniques, *NDT and E Int.* 38 (8) (2005) 682–689.
- [25] M.A. Pech-Canul, P. Castro, Corrosion measurements of steel reinforcement in concrete exposed to a tropical marine atmosphere, *Cem. Concr. Res.* 32 (3) (2002) 491–498.
- [26] S. Kakooei, H.M. Akil, A. Dolati, J. Rouhi, The corrosion investigation of rebar embedded in the fibers reinforced concrete, *Constr. Build. Mater.* 35 (2012) 564–570.
- [27] T. Korouzhdeh, H. Eskandari-Naddaf, Cost-safety optimization of steel-concrete composite beams using standardized formulation, *Engineering Science and Technology, an International Journal* 22 (2) (2019) 523–532.
- [28] S. Mahdiniya, H. Eskandari-Naddaf, R. Shadnia, Effect of cement strength class on the prediction of compressive strength of cement mortar using GEP method, *Constr. Build. Mater.* 198 (2019) 27–41.
- [29] M. Momeni, M.H. Moayed, A. Davoodi, Tuning DOS measuring parameters based on double-loop EPR in H₂SO₄ containing KSCN by Taguchi method, *Corros. Sci.* 52 (8) (2010) 2653–2660.
- [30] A. Joshaghani, A.A. Ramezani-pour, O. Ataei, A. Golroo, Optimizing pervious concrete pavement mixture design by using the Taguchi method, *Constr. Build. Mater.* 101 (2015) 317–325.
- [31] M.A. DeRousseau, J.R. Kasprzyk, W.V. Srubar III, Computational design optimization of concrete mixtures: A review, *Cem. Concr. Res.* 109 (2018) 42–53.
- [32] M. Sonebi, Medium strength self-compacting concrete containing fly ash: Modelling using factorial experimental plans, *Cem. Concr. Res.* 34 (7) (2004) 1199–1208.
- [33] S. Damiri, H.R. Pouretdal, O. Bakhshi, An extreme vertices mixture design approach to the optimization of methylal production process using p-toluenesulfonic acid as catalyst, *Chem. Eng. Res. Des.* 112 (2016) 155–162.
- [34] F. Bendebane, L. Bouziane, F. Ismail, Liquid-liquid Extraction of Naphthalene. Application of a Mixture Design and Optimization, *Energy Procedia* 36 (2013) 1241–1248.
- [35] J.-T. Ding, P.-Y. Yan, S.-L. Liu, J.-Q. Zhu, Extreme vertices design of concrete with combined mineral admixtures, *Cem. Concr. Res.* 29 (6) (1999) 957–960.

- [36] Huang, W.R., et al. Permeability of Concrete Containing Air-Entraining and Mineral Admixtures. in *Advanced Materials Research*. 2011. Trans Tech Publ
- [37] H. Eskandari-Naddaf, R. Kazemi, ANN prediction of cement mortar compressive strength, influence of cement strength class, *Constr. Build. Mater.* 138 (2017) 1–11.
- [38] N.M. Al-Akhras, Durability of metakaolin concrete to sulfate attack, *Cem. Concr. Res.* 36 (9) (2006) 1727–1734.
- [39] K.C. Hover, R.J. Phares, Impact of Concrete Placing Method on Air Content, Air-Void System Parameters, and Freeze-Thaw Durability, *Transp. Res. Rec.* 1532 (1) (1996) 1–8.
- [40] A. Madadi, H. Eskandari-Naddaf, R. Shadnia, L. Zhang, Characterization of ferrocement slab panels containing lightweight expanded clay aggregate using digital image correlation technique, *Constr. Build. Mater.* 180 (2018) 464–476.
- [41] M. Ghaemi-Fard, H. Eskandari-Naddaf, G.R. Ebrahimi, Genetic prediction of cement mortar mechanical properties with different cement strength class after freezing and thawing cycles, *Structural Concrete* 19 (5) (2018) 1341–1352.
- [42] A. Kargari, H. Eskandari-Naddaf, R. Kazemi, Effect of cement strength class on the generalization of Abrams' law, *Structural Concrete* 20 (1) (2019) 493–505.
- [43] T.A. Van-Loc, T. Senga Kiese, S. Bonnet, A. Ventura, Application of sensitivity analysis in the life cycle design for the durability of reinforced concrete structures in the case of XC4 exposure class, *Cem. Concr. Compos.* 87 (2018) 53–62.
- [44] Neville, A.M., *Properties of concrete*. Vol. 4. 1995: Longman London.
- [45] ASTM, Standard test method for determining the percentage of fractured particles in coarse aggregate. 2013.
- [46] ASTM, C., 494. Standard specification for chemical admixtures for concrete, 1999. 4
- [47] Standard, A., C136/C136M-14, 2015. Standard Test Method for Sieve Analysis of Fine and Coarse Aggregates, 2014.
- [48] ASTM, C., 260. Standard Specification for Air-Entraining Admixtures for Concrete. 2001, West Conshohocken, PA: ASTM International.
- [49] A.M. Neville, *Properties of Concrete* 687: (2011) 331.
- [50] Hesam Madani, Alireza Bagheri, Tayebeh Parhizkar, Amirniaziar Raisghasemi, Chloride penetration and electrical resistivity of concretes containing nanosilica hydrosols with different specific surface areas, *Cem. Concr. Compos.* 53 (2014) 18–24.
- [51] D. John, P. Searson, J. Dawson, Use of AC impedance technique in studies on steel in concrete in immersed conditions, *Br. Corros. J.* (2013).
- [52] Brian B. Hope, John A. Page, Alan K.C. Ip, Corrosion rates of steel in concrete, *Cem. Concr. Res.* 16 (5) (1986) 771–781.
- [53] Leila Hachani, Juan Carpio, Christian Fiaud, André Raharinaivo, Ezzedine Triki, Steel corrosion in concretes deteriorated by chlorides and sulphates: Electrochemical study using impedance spectrometry and 'stepping down the current' method, *Cem. Concr. Res.* 22 (1) (1992) 56–66.
- [54] P. Gu et al., Performance of Steel Reinforcement in Portland Cement and High-Volume Fly Ash Concretes, *ACI Mater. J.* 96 (5) (1999).
- [55] Ha-Won Song, Jong-Chul Jang, Velu Saraswathy, Keun-Joo Byun, An estimation of the diffusivity of silica fume concrete, *Build. Environ.* 42 (3) (2007) 1358–1367.
- [56] M.F. Montemor, A.M.P. Simões, M.G.S. Ferreira, Chloride-induced corrosion on reinforcing steel: from the fundamentals to the monitoring techniques, *Cem. Concr. Compos.* 25 (4-5) (2003) 491–502.
- [57] S.J. Ford, J.D. Shane, T.O. Mason, Assignment of features in impedance spectra of the cement-paste/steel system, *Cem. Concr. Res.* 28 (12) (1998) 1737–1751.
- [58] Lay, P., et al., An ac impedance study of steel in concrete. *Journal of applied electrochemistry*, 1985. 15(5): p. 755–766
- [59] Madej, D., A new implementation of electrochemical impedance spectroscopy (EIS) and other methods to monitor the progress of hydration of strontium monoaluminate (SrAl₂O₄) cement. *Journal of Thermal Analysis and Calorimetry*: p. 1–12.
- [60] L. Bertolini et al., *Corrosion of Steel in Concrete: Prevention, Diagnosis, Repair*, 2004.
- [61] Broomfield, J.P., *Corrosion of steel in concrete: understanding, investigation and repair*. 2003: CRC Press.
- [62] Saeid Ghorbani, Iman Tajji, Mohammadreza Tavakkolizadeh, Ali Davodi, Jorge de Brito, Improving corrosion resistance of steel rebars in concrete with marble and granite waste dust as partial cement replacement, *Constr. Build. Mater.* 185 (2018) 110–119.
- [63] Zheng Liu, J.J. Beaudoin, An assessment of the relative permeability of cement systems using AC impedance techniques, *Cem. Concr. Res.* 29 (7) (1999) 1085–1090.
- [64] A. Standard, Standard test method for sieve analysis of fine and coarse aggregates, West Conshohocken, PA, USA, ASTM International, 1998.
- [65] L. Valek, S. Martinez, D. Mikulić, I. Brnardić, The inhibition activity of ascorbic acid towards corrosion of steel in alkaline media containing chloride ions, *Corros. Sci.* 50 (9) (2008) 2705–2709.
- [66] Monica Farcas, Nicholas P. Cosman, David K. Ting, Sharon G. Roscoe, Sasha Omanovic, A comparative study of electrochemical techniques in investigating the adsorption behaviour of fibrinogen on platinum, *J. Electroanal. Chem.* 649 (1-2) (2010) 206–218.
- [67] ASTM, C., Standard test method for density, absorption, and voids in hardened concrete. C642-13, 2013
- [68] L.G. Li, J.Y. Zheng, J. Zhu, A.K.H. Kwan, Combined usage of micro-silica and nano-silica in concrete: SP demand, cementing efficiencies and synergistic effect, *Constr. Build. Mater.* 168 (2018) 622–632.
- [69] F.U.A. Shaikh, Y. Shafaei, P.K. Sarker, Effect of nano and micro-silica on bond behaviour of steel and polypropylene fibres in high volume fly ash mortar, *Constr. Build. Mater.* 115 (2016) 690–698.
- [70] Ehsan Ghafari, Mahdi Arezoumandi, Hugo Costa, Eduardo Júlio, Influence of nano-silica addition on durability of UHPC, *Constr. Build. Mater.* 94 (2015) 181–188.
- [71] Ueli M. Angst, Challenges and opportunities in corrosion of steel in concrete, *Mater Struct* 51 (1) (2018), <https://doi.org/10.1617/s11527-017-1131-6>.
- [72] M. Stefanoni, U.M. Angst, B. Elsener, Electrochemistry and capillary condensation theory reveal the mechanism of corrosion in dense porous media, *Sci. Rep.* 8 (1) (2018) 1–10.
- [73] Marijana Serdar, Stéphane Poyet, Valérie L'Hostis, Dubravka Bjegović, Carbonation of low-alkalinity mortars: Influence on corrosion of steel and on mortar microstructure, *Cem. Concr. Res.* 101 (2017) 33–45.
- [74] S. Gavela, A. Ntziouni, E. Rakanta, N. Kouloumbi, V. Kasselouri-Rigopoulou, Corrosion behaviour of steel rebars in reinforced concrete containing thermoplastic wastes as aggregates, *Constr. Build. Mater.* 41 (2013) 419–426.
- [75] Jing Ming, Jinjie Shi, Wei Sun, Effect of mill scale on the long-term corrosion resistance of a low-alloy reinforcing steel in concrete subjected to chloride solution, *Constr. Build. Mater.* 163 (2018) 508–517.
- [76] Han-Seung Lee, Hyun-Min Yang, Jitendra Kumar Singh, Shailesh Kumar Prasad, Bongyoung Yoo, Corrosion mitigation of steel rebars in chloride contaminated concrete pore solution using inhibitor: An electrochemical investigation, *Constr. Build. Mater.* 173 (2018) 443–451.
- [77] Kangkang Tang, Stray current induced corrosion of steel fibre reinforced concrete, *Cem. Concr. Res.* 100 (2017) 445–456.
- [78] Dif Fodil, Mouli Mohamed, Compressive strength and corrosion evaluation of concretes containing pozzolana and perlite immersed in aggressive environments, *Constr. Build. Mater.* 179 (2018) 25–34.
- [79] Shishir Mundra, Maria Criado, Susan A. Bernal, John L. Provis, Chloride-induced corrosion of steel rebars in simulated pore solutions of alkali-activated concretes, *Cem. Concr. Res.* 100 (2017) 385–397.
- [80] L Holloway, K Nairn, M Forsyth, Concentration monitoring and performance of a migratory corrosion inhibitor in steel-reinforced concrete, *Cem. Concr. Res.* 34 (8) (2004) 1435–1440.
- [81] Mohamed Ismail, Masayasu Ohtsu, Corrosion rate of ordinary and high-performance concrete subjected to chloride attack by AC impedance spectroscopy, *Constr. Build. Mater.* 20 (7) (2006) 458–469.
- [82] Hamid Eskandari, Alireza Mozafari Nic, Anis Ghanei, Effect of Air Entraining Admixture on Corrosion of Reinforced Concrete, *Procedia Eng.* 150 (2016) 2178–2184.
- [83] M.S. Software, Minitab Reference Manual, Minitab Inc., State College, PA, 2017.
- [84] Amirhossein Madadi, Mahdi Tasdighi, Hamid Eskandari-Naddaf, Structural response of ferrocement panels incorporating lightweight expanded clay and perlite aggregates: Experimental, theoretical and statistical analysis, *Eng. Struct.* 188 (2019) 382–393.
- [85] A. Ghanei, H. Eskandari-Naddaf, A. Davoodi, Corrosion behavior and optimization of air-entrained reinforced concrete, incorporating microsilica, *Structural Concrete* 19 (5) (2018) 1472–1480.